LBL-31453
Preprint

Lawrence Berkeley Laboratory
UNIVERSITY OF CALIFORNIA

Materials & Chemical Sciences Division

Submitted to the Journal of the American Ceramic Society

**Rare-Earth Disilicate–Silicon Nitride Ceramics:
I. Design, Fabrication, and Secondary-Phase Crystallization**

M.K. Cinibulk, G. Thomas, and S.M. Johnson

November 1991

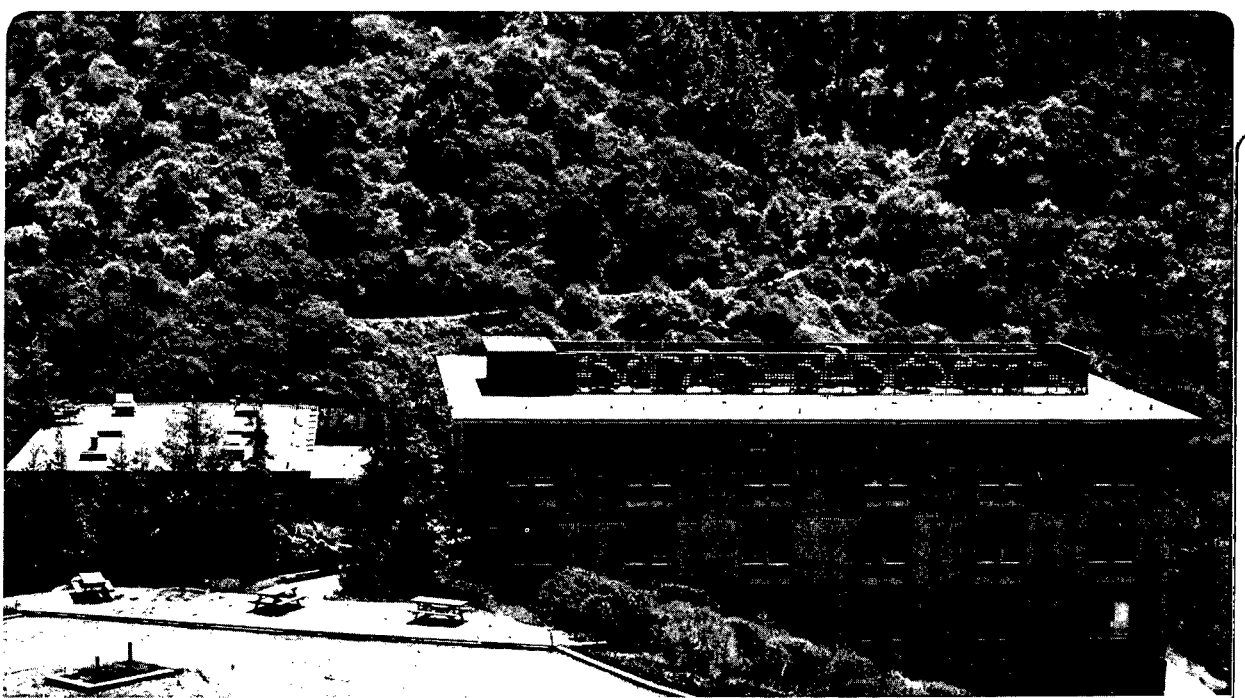

Prepared for the U.S. Department of Energy under Contract Number DE-AC03-76SF00098

DISCLAIMER

DISCLAIMER

LBL-31453

Rare-Earth Disilicate–Silicon Nitride Ceramics: I. Design, Fabrication, and Secondary-Phase Crystallization

Michael K. Cinibulk[#*] and Gareth Thomas[#]

Department of Materials Science and Mineral Engineering
University of California
and
Center for Advanced Materials
Materials Sciences Division
Lawrence Berkeley Laboratory
University of California
Berkeley, California 94720

Sylvia M. Johnson[#]

Materials Research Laboratory
SRI International
Menlo Park, CA 94025

November 1991

[#]Member, American Ceramic Society
[*]Currently with Max-Planck-Institut für Metallforschung, Stuttgart, FRG

This work was supported in part by the National Science Foundation under Contract No. DMR 83-1317239 and by the Director, Office of Energy Research, Office of Basic Energy Sciences, Materials Sciences Division, of the U.S. Department of Energy under Contract No. DE-AC03-76SF00098.

Abstract

The fabrication and intergranular-phase devitrification of silicon nitride densified with rare-earth (RE) oxide additives has been investigated. The additions of the oxides of Sm, Gd, Dy, Er, and Yb, having high melting points and behaving similarly to Y_2O_3, were compositionally controlled to tailor a microstructure with a crystalline secondary phase of $RE_2Si_2O_7$. The lanthanide oxides were found to be as effective as Y_2O_3 in densifying Si_3N_4, resulting in identical microstructures and densities of 98-99% of theoretical density. The crystallization behavior of all six disilicates was similar, characterized by a limited nucleation and rapid growth mechanism resulting in large single crystals. Complete crystallization of the intergranular phase was obtained with the exception of a thin residual amorphous film which was observed at interfaces and believed to be rich in impurities, the cause of incomplete devitrification. [Key Words: crystallization, microstructure, processing, rare-earth oxides, silicon nitride.]

I. Introduction

Silicon nitride ceramics are currently being considered for use as structural components in high-temperature oxidizing environments. High resistance to thermal shock, along with high strength, high fracture toughness, and high resistance to chemical attack makes silicon nitride a suitable material for components operating under extreme conditions. In these applications, the thermomechanical response of the ceramic to external forces depends on the microstructure and phase composition, in particular on the refractoriness and chemical activity of the constituent phases. Conventional Si_3N_4 ceramics consist of highly refractory grains bonded by a less refractory vitreous phase. Therefore, the high-temperature behavior depends primarily on the composition, distribution, and state of the intergranular phase. Silicon nitride itself is extremely oxidation resistant due to the protective SiO_2 layer, which results from exposure to high

oxygen partial pressures at elevated temperatures.[1] However, high-temperature exposure of silicon nitride sintered with oxide additives leads to accelerated oxidation attributable to the enhanced oxidation of Si_3N_4 dissolved in a highly viscous silicate phase present at the surface.[1] Since diffusion of additive and impurity cations through an amorphous grain-boundary phase from the bulk to the surface oxide scale is rate limiting[2], obtaining refractory crystalline phases in equilibrium with SiO_2 should eliminate the driving force for cation diffusion and improve oxidation resistance. Devitrification of the intergranular phase can also result in materials with improved high-temperature strength and creep resistance.

Of the possible silicates and oxynitrides that can form as secondary phases in Si_3N_4 ceramics fabricated in the Si_3N_4-SiO_2-Y_2O_3 system, shown in Fig. 1, $Y_2Si_2O_7$ is the phase that is most resistant to oxidation.[3] $Y_2Si_2O_7$ is the only Y-containing phase in equilibrium with SiO_2, the oxidation product of Si_3N_4, and is therefore the preferred secondary phase for Si_3N_4 ceramics which will be exposed to high-temperature oxidizing environments. Under these conditions the other possible secondary phases oxidize to $Y_2Si_2O_7$, SiO_2, and N_2; these reactions are accompanied by volumetric changes and gas evolution leading to stresses that may eventually result in cracking and failure of the ceramic.

In addition to yttrium disilicate, the disilicates of the lanthanides should also prove effective for the formation of refractory Si_3N_4 ceramics. Limited work has been published on the use of lanthanide oxides as sintering additives for Si_3N_4.[4-12] These studies have focused primarily on sintering feasibility and behavior of the ceramics with the lighter lanthanide oxides (oxides of La, Ce, Nd, or Sm). These oxides were found to be nearly as effective as Y_2O_3 in densifying Si_3N_4, producing materials having slightly lower room-temperature strengths and slightly higher strengths at 1370°C.[9]

Phase relations in the Si_3N_4-SiO_2-RE_2O_3 system are generally not well known for the majority of the lanthanide oxides (here, RE refers to Y, as well as the elements collectively known as lanthanides, La→Lu), however, they are generally regarded to be

similar to those in the Si_3N_4-SiO_2-Y_2O_3 system. The lanthanide ions all have similar electronic configurations and ionic radii, with RE^{3+} being the common oxidation state, and therefore the chemistry within of the group is very similar as well. In rare-earth aluminosilicate glasses it has been shown that yttrium behaves similarly to the lanthanides in forming melts.[13] The physical properties of these glasses such as glass transformation and softening temperatures, and thermal expansion coefficient varied linearly with ionic radius for the rare-earth ions; this trend was attributed to the field strength of the rare-earth ion (field strength varies with the reciprocal of cationic radius). Ito and Johnson[14] and Felsche[15] have shown that phases in the RE_2O_3-SiO_2 system and the Y_2O_3-SiO_2 system are isostructural, forming silicates having the general formulae RE_2SiO_5 and $RE_2Si_2O_7$. The formation of isostructural silicon lanthanide oxynitrides has also been demonstrated.[16]

In this paper the fabrication and intergranular-phase crystallization of Si_3N_4 sintered with Y_2O_3, as well as the heavier lanthanide oxides (oxides of Sm, Gd, Dy, Er, or Yb), is described. The high-temperature behavior of these materials has been evaluated as well and will be discussed in subsequent papers.[17,18] These lanthanide oxides all have eutectic temperatures with SiO_2 of 1640-1680°C, about the same as that of Y_2O_3-SiO_2 (1660°C) indicating they should form highly refractory grain-boundary phases. The crystallization behavior of these compounds is also expected to be similar to those of the Si_3N_4-SiO_2-Y_2O_3 system. Although complete crystallization of the intergranular phase is ideal it has been proposed based on thermodynamical considerations[19] (and also generally observed) that a thin residual amorphous film, will always exist at grain boundaries. Therefore, the use of the higher melting point rare-earth oxides as sintering aids, would also provide a highly refractory (viscous) amorphous phase should complete devitrification not be achieved.

II. Experimental Procedure

(1) Material Fabrication

To fabricate silicon nitride ceramics with high strength while maintaining high oxidation resistance, it is important to stay compositionally as close to the Si_3N_4-$Y_2Si_2O_7$ tie-line as possible. Materials with an overall composition in the upper left portion of the Si_3N_4-Si_2ON_2-$Y_2Si_2O_7$ compatibility triangle (Fig. 1) contain significant fractions of Si_2ON_2, a more oxidation resistant but lower strength phase than Si_3N_4.[20,21] Alternatively, if the composition crosses the Si_3N_4-$Y_2Si_2O_7$ tie-line into the Si_3N_4-$Y_2Si_2O_7$-$Y_{10}Si_7O_{23}N_4$ compatibility triangle, the apatite ($Y_{10}Si_7O_{23}N_4$) phase which is not in equilibrium with SiO_2 can exist resulting in increased oxidation results. Compositions were therefore carefully controlled to result in a final product lying directly on the Si_3N_4-$RE_2Si_2O_7$ tie-line.

Si_3N_4 powder†, obtained directly from the manufacturer, was selected for use in this research primarily because of its high purity, high specific surface area (11.5 m^2/g) and high α/β content (>95%). Major impurities common to silicon nitride powders including aluminum, calcium, and iron were reported to be <100 ppm. Oxide sintering additives used were Y_2O_3§, SiO_2¶, and rare-earth oxides**. The rare-earth oxides selected to be examined as sintering additives were the heavier and more refractory lanthanide oxides: Sm_2O_3, Gd_2O_3, Dy_2O_3, Er_2O_3, and Yb_2O_3. The oxides of those lanthanides that were not included in this study lying between samarium and lutetium were omitted because of their prohibitively high cost and limited availability.

All Si_3N_4 compositions were prepared with a 2:1 molar ratio of SiO_2:RE_2O_3 (taking into account oxide present on the surface of Si_3N_4 particles), placing the composition directly on the Si_3N_4-$RE_2Si_2O_7$ tie line. Care was taken in handling the Si_3N_4 powder so as to prevent additional oxidation. Materials were processed to obtain a 12.3 vol% grain-boundary phase for all compositions; this volume fraction is equivalent to

a 15 wt% $Y_2Si_2O_7$-Si_3N_4 material, which was found to sinter to >99 % theoretical density. Table I summarizes the compositions of each material fabricated.

The compositions were prepared by milling the powders using Si_3N_4 milling media (~3.2mm diameter) in anhydrous methanol. The dried powders were then sieved, and lightly die-pressed into rectangular shapes. The shapes were then immediately cold isostatically pressed to obtain maximum green densities and to minimize density gradients which may have been introduced during uniaxial pressing. The samples were placed in a bed of 30 wt% BN-Si_3N_4 powder in a BN-coated graphite crucible and sintered in a graphite-element furnace at 1850°C for 4 hr under 1.8 MPa N_2. Following densification, the furnace was cooled to 1400°C and held for 24 hr to devitrify the intergranular phase. Theoretical densities were calculated assuming a fully crystalline grain-boundary phase of the appropriate $RE_2Si_2O_7$ and using the rule of mixtures. Actual bulk densities were determined by the Archimedes method of weighing the sample in air and then in ethanol, which was used as the immersion liquid.

(2) Microstructural Characterization

X-ray diffraction was used to identify major secondary crystalline phases present in the ceramics, which were scanned in bulk using Cu Kα radiation. Each of the samples was examined by reflected light microscopy for porosity and homogeneity, including evidence of secondary-phase segregation. The microstructures of the final devitrified Si_3N_4 materials were examined in a transmission electron microscope[††] operated at 120 kV and equipped with an energy-dispersive x-ray spectrometer[§§] incorporating an ultra-thin window detector for analysis of elements with atomic number ≥5. Electron diffraction was used to identify secondary crystalline and amorphous phases. Dark-field imaging using both diffracted electrons and incoherently scattered electrons was used to image crystalline and amorphous phases, respectively. Specimens for TEM were prepared by ion beam thinning to achieve electron transparency. A thin layer of carbon was then evaporated onto the specimens to minimize charging under the electron beam.

III. Results

(1) Processing

All ceramics appeared smooth and uniform with no evidence of warping or cracking upon consolidation into the final green state. The green densities of all consolidated powders were ~58% of theoretical density. The densities of the final sintered samples are included in Table I, with the dimensions being 4.5 mm x 15 mm x 45 mm, from which flexure test specimens could be machined. Sintered densities ranged from 98.0% for the Sm_2O_3-sintered Si_3N_4 to 99.8% of theoretical density for the Gd_2O_3-sintered Si_3N_4. Most of the sintered samples were dark gray in color with the Sm_2O_3-sintered Si_3N_4 having a violet-gray coloring and the Er_2O_3-sintered Si_3N_4 having a slightly reddish-gray coloring (Er_2O_3 powder is pink). The compositions lost 3.5-6% in weight depending on the specific composition following sintering, which can be attributed to loss of adsorbed water as well as partial decomposition of Si_3N_4 and reduction of SiO_2 to SiO.

(2) Microstructural Characterization

(A) X-ray Diffraction of Bulk Materials: All x-ray diffraction patterns of the bulk sectioned samples consisted of well defined peaks with no evidence of incoherent scattering of x-rays that would indicate the presence of a high amorphous phase content. Table II contains the identification of crystalline phases identified by x-ray diffraction. Only the β-phase of Si_3N_4 was detected along with the possibility of trace amounts of Si_2ON_2, indicating the final compositions were slightly inside the Si_3N_4-Si_2ON_2-$RE_2Si_2O_7$ compatibility triangle. This small deviation from the Si_3N_4-$RE_2Si_2O_7$ tie-line can be attributed to greater amounts of impurity oxide present on the Si_3N_4 powders than specified by the manufacturer resulting from the continuous oxidation of Si_3N_4 during handling, as well as additional oxidation of Si_3N_4 occurring during processing to the green state.

The rare-earth disilicates in most of the compositions were crystallized at 1400°C in the forms predicted and experimentally determined by previous investigators.[14,15,22] The

Y_2O_3-, Sm_2O_3-, Er_2O_3-, and Yb_2O_3-sintered Si_3N_4 ceramics contained secondary phases of β-$Y_2Si_2O_7$, *A*-$Sm_2Si_2O_7$, β-$Er_2Si_2O_7$, and β-$Yb_2Si_2O_7$, respectively, as expected (the use of capital letters to denote the various polymorphs of the rare-earth disilicates was used by Felsche[15], while the use of Greek letters was adopted by Ito and Johnson[14] for the polymorphs of $Y_2Si_2O_7$. The latter convention has been chosen here for all rare-earth disilicates where applicable). $Gd_2Si_2O_7$ and $Dy_2Si_2O_7$ crystallized in the δ-phase, with lesser amounts of α-$Dy_2Si_2O_7$ also detected, whereas the α-phase had been reported as the stable polymorph for both at 1400°C.[14,15]

(B) TEM of Secondary Phases: Fig. 2 presents a set of low-magnification transmission electron micrograph showing the general morphologies of the six compositions, with the β-Si_3N_4 grains in bright contrast and the rare-earth disilicate phase in much darker contrast due to the higher average atomic number of the secondary phase. The general morphologies of the microstructures of the six compositions were very similar. The secondary phase was observed primarily at multiple-grain junctions, with a thin layer at times along two-grain boundaries.

Fig. 3 shows the microstructure of the $Y_2Si_2O_7$-Si_3N_4 composition. The dark-field image, obtained by using one of the diffracted electron beams from the β-$Y_2Si_2O_7$ diffraction pattern, reveals the crystalline β-$Y_2Si_2O_7$ phase in bright contrast. Single crystals of $RE_2Si_2O_7$ extending over several square micrometers was commonly observed in all six compositions, indicating a similar limited-nucleation/rapid-growth mechanism of this phase. Such crystallization behavior has been reported in Si_3N_4 ceramics containing secondary phases of $Y_2Si_2O_7$,[23,24] and $YSiO_2N$ and $Y_4Si_2O_7N_2$,[24] as well as $Y_3Al_5O_{12}$.[25] β-$Y_2Si_2O_7$ was the only polymorph indicated by electron diffraction in the $Y_2Si_2O_7$-Si_3N_4 material. All the multi-grain junctions analyzed by TEM appeared to have completely crystallized. Imaging of amorphous films in these ceramics was extremely difficult due to the low intensity of electrons diffusely scattered by the minimal volume fraction of amorphous phase. The existence of a thin residual amorphous film was only

detected at the interfaces of $Y_2Si_2O_7$ and Si_3N_4 grains and at Si_3N_4-Si_3N_4 grains by diffuse dark-field imaging as shown in Fig. 4.

The microstructures of the other $RE_2Si_2O_7$-Si_3N_4 ceramics were very similar to those of the $Y_2Si_2O_7$-Si_3N_4 material. However, due to the presence of the rare-earth elements in the secondary phases, resulting in high electron scattering and absorption, extremely dark contrast of this phase was obtained in all orientations (Fig. 2). Obtaining diffraction patterns with a convergent beam and obtaining crystalline images in bright contrast in dark field was therefore complicated and limited to only the thinnest portions of the specimen where adequate electron transparency existed.

The intergranular phases were otherwise identical in appearance to those of the $Y_2Si_2O_7$-Si_3N_4 material, with complete crystallization of secondary phases at multiple-grain junctions observed in all but the $Yb_2Si_2O_7$-Si_3N_4 material. Fig. 5 shows dark-field images of the $Sm_2Si_2O_7$-Si_3N_4 and $Er_2Si_2O_7$-Si_3N_4 compositions indicating similar crystallization and growth mechanisms operating for each material. One composition, $Yb_2Si_2O_7$-Si_3N_4 contained a small amount of residual amorphous phase at the multiple-grain junctions in an isolated area of the TEM specimen. The partially crystallized multiple-grain junctions were observed in only a small region of the specimen, while the other regions consisted of fully crystalline β-$Yb_2Si_2O_7$ as the secondary phase. The amorphous phase appeared in somewhat brighter contrast than β-$Yb_2Si_2O_7$ and often contained gas bubbles characteristic of radiation damage, from either ion milling during specimen preparation or the electron beam *in situ*.[28,29]

Energy-dispersive x-ray spectroscopy of this amorphous phase indicated a much higher concentration of silicon than that detected in β-$Yb_2Si_2O_7$, which is primarily why the glass is slightly more transparent. Impurities commonly expected to reside in the amorphous grain-boundary phases of Si_3N_4 ceramics, such as Mg, Al, Ca, and Fe, were not detected in appreciable concentrations in the amorphous Yb-Si-O-N phase. The detection of small amounts of Al, however, is also complicated by the presence of Yb since

the location of the Yb Mα peak obscures the Al Kα peak. The observation of this amorphous phase in only an isolated region of the specimen rather than in a random or even distribution throughout the microstructure, and the presence of excess silicon but not impurity transition metals in this phase implies that this region where the two secondary phases (β-$Yb_2Si_2O_7$ and Yb-Si-O-N glass) exist resulted from the presence of excess SiO_2, possibly in the form of inclusions of large SiO_2 particles that were not reduced during milling.

Analysis of the β-Si_3N_4 grains in all materials indicated the presence of only Si, N, and O (present as a surface-oxide impurity); i.e., the rare-earths do not exist as substitutional impurities in Si_3N_4 due to their large ionic radii (~0.86-0.96 Å)[15]. However, iron-rich particles were observed to occur within Si_3N_4 grains and also at the grain boundaries. Fig. 6 contains a bright-field image of Fe-rich inclusions in the $Yb_2Si_2O_7$-Si_3N_4 material. Iron has been reported to have been detected exclusively as small crystalline particles in oxynitride glasses[26,30] and in the glassy grain-boundary phases of silicon nitride ceramics.[31] These particles have been cited as nucleation centers for β-Si_3N_4 as well as for secondary-phase crystals.[26,32] Fig. 6(b) shows the EDS spectra obtained from the inclusion at the center of the Si_3N_4 grain in the $Yb_2Si_2O_7$-Si_3N_4 material. In addition to Fe, impurities of Cr and Ti were detected within these particles, as well as Si and Yb.

Microanalysis of the secondary phase rare-earth disilicates in all materials revealed only the presence of Si, O, and the appropriate rare-earth atom. Detection of compositional changes due to the presence of amorphous phases at the grain boundaries was attempted.However, due to the thin width and improbability of obtaining a grain-boundary in an edge-on orientation at the fixed angle of specimen tilt required for x-ray acquisition no compositional variations were detectable between grains and grain-boundaries.

IV. Discussion

(1) Crystallization of the Intergranular Phase

The densification of Si_3N_4 ceramics produced by sintering in the presence of a liquid has been described by Kingery[33] as being caused by compressive forces, arising from capillary pressure, acting between particles that are in contact. These compressive forces give rise to the higher solubility of the Si_3N_4 particles at the contact positions. The diffusion of Si_3N_4 in the liquid phase away from the points of contact, leads to densification. The question of whether there is intimate contact of the particles resulting in a final microstructure where Si_3N_4 grains could be in direct contact with the expulsion of all liquid from two-grain boundaries to the multiple-grain junctions has been addressed by Lange.[34] By applying a theory developed for plates that sandwich a liquid layer to that of spherical particles undergoing liquid-phase sintering, it was predicted that although the liquid layer decreases with time, a finite thickness will always remain between particles when the liquid perfectly wets the solid. In fact microscopy studies have verified the existence of thin intergranular amorphous films existing in sintered Si_3N_4 (for example Refs. 35-37).

Clarke[38] subsequently discussed whether thin intergranular films can adopt an equilibrium thickness in polycrystalline ceramics. It was shown, based on interfacial energies and on the force balance normal to the grain boundary, that the origin of an equilibrium thickness was the result of two competing interactions.These ineractions of an attractive van der Waals dispersion force between the grains on either side of the boundary acting to thin the film and a repulsive force due to the structure of the liquid opposing this attraction. An equilibrium thickness on the order of 1 nm was proposed based on the short range of these interactions, but being ultimately dependent on the composition of the liquid, as well as that of the grains on either side of the liquid.

To date, crystallization of the intergranular liquid in Si_3N_4 ceramics has always resulted in a residual amorphous phase residing at both two-grain junctions as thin films

and at multiple-grain junctions, typically segregated at the nodes. Raj and Lange[19] have shown that complete crystallization of the amorphous phase segregated in grain boundaries in polyphase ceramics is more difficult to achieve than crystallization of the same phase in bulk. Their calculations have shown that liquid constrained in the grain boundaries may support hydrostatic stresses and any volume changes occuring during phase transformation, therefore, will give rise to strain energy which will oppose devitrification.

Other factors complicating complete crystallization of the intergranular phase include compositional inhomogeneties and the presence of impurities which segregate to this phase from the starting powders during the solution-reprecipitation process. The presence of compositional heterogeneities in the intergranular glass can lead to regions with enhanced glass stability, resulting in only partial devitrification of multiple-grain junctions in these regions. The enhanced stability of amorphous phases and their subsequent resistance to devitrification have also been attributed to the presence of impurities.[39] The stabilization of vitreous materials by the addition of network forming impurities is a common practice in the industry.[40]

(2) Crystallization of $RE_2Si_2O_7$ as a Secondary Phase

The crystallization behavior of $RE_2Si_2O_7$ at the multiple-grain junctions of these compositions consists of large scale crystal growth exceeding the single multiple-grain junction where nucleation occurred. Single crystals have been shown to span several micrometers (Fig. 3). Work in crystallizing other Si_3N_4 compositions also resulted in a similar secondary phase morphology.[23-25] While Bonnell et al.[24] observed the crystallization behavior of yttrium aluminum garnet ($Y_3Al_5O_{12}$) in sialon ceramics to proceed via large scale growth of single crystals, crystallization of cordierite ($Mg_2Al_4Si_5O_{14}$) resulted in a fine-grained structure with each multiple-grain junction composed of individual crystals. The crystallization behavior resulting in the differing secondary-phase morphologies is a function of the relative ease of nucleation versus growth of the crystals. For the crystallization of a phase where nucleation is limited,

growth proceeds from fewer nuclei resulting in a secondary phase consisting of fewer but larger grains. The crystallization of a phase undergoing frequent nucleation events, results in a secondary phase consisting of many fine grained crystals.

The processing of the materials in the present study entailed a drop from the sintering temperature directly to the temperature where crystallization occurred. The absence of a nucleation period at a temperature just above the softening point of the glass decreases possibly to zero the nucleation rate becaause since at the higher temperatures the solubility in the melt is maximized. By incorporating a two-stage heat treatment, maximum rates of nucleation and growth may be realized[40], resulting in a finer grained microstructure with possibly improved fracture strength but reduced creep resistance.[41] An alternative method to obtain a finer dispersion of secondary-phase grains would be to incorporate chemically inert particles (such as ZrO_2) as nucleating agents into the sintering additives.[39] The type of secondary-phase morphology required is dependent on the material properties desired. The observation that all materials in this study exhibited similar secondary-phase crystallization behavior was expected from previous work on the formation of the rare-earth disilicates in bulk.[14,15]

V. Conclusions

The additions of the oxides of Y, Sm, Gd, Dy, Er, and Yb were compositionally controlled to tailor a microstructure consisting of a β-Si_3N_4 discontinuous matrix phase and a crystalline secondary phase of $RE_2Si_2O_7$. Based on the microstructural observations obtained by x-ray diffraction and transmission electron microscopy, the following conclusions can be made:

(1) The lanthanide oxides studied in this investigation as sintering additives for silicon nitride have been shown to be as effective as Y_2O_3 in densifying Si_3N_4 by sintering without the aid of an applied stress (i.e., hot-pressing or hot-isostatic pressing). Densities of 98-99% theoretical density were achieved with 2:1 SiO_2-RE_2O_3 additives of 12.3 vol%

for all compositions. The $Sm_2Si_2O_7$-Si_3N_4 and $Er_2Si_2O_7$-Si_3N_4 materials contained the most porosity.

(2) The appropriate rare-earth disilicate was obtained following devitrification at 1400°C. The morphologies of the microstructures of the six compositions were identical with high aspect ratio β-Si_3N_4 grains as the primary phase and a secondary phase consisting of large grained $RE_2Si_2O_7$. The crystallization behavior of all six disilicates was similar, characterized by a limited nucleation and rapid growth mechanism resulting in large single crystals as the secondary phase.

(3) Complete crystallization of the intergranular phase was obtained with the exception of a thin (1-10 nm) residual amorphous film, which was observed at interfaces and is believed to be rich in impurities that were initially present in the Si_3N_4 and SiO_2 starting powders, and which inhibit complete devitrification. The $Yb_2Si_2O_7$-Si_3N_4 material contained isolated regions of incompletely crystallized multiple grain junctions, due to compositional heterogeneities in the milled Si_3N_4-SiO_2-Yb_2O_3 powder. No impurities were detected in these amorphous regions or at the two-grain interfaces13, although Fe-rich particles were observed at grain boundaries and also within β-Si_3N_4 grains themselves.

(4) Constraints due to both thermodynamics and the presence of impurities seem to be responsible for stabilizing a residual amorphous phase in which the concentration of the impurities increases as they are excluded from the regions where devitrification occurs.

† Type SN E-10, Ube Industries, Tokyo, Japan

§ 99.9%, 1 μm, Hermann C. Starck Co., Berlin, Germany

¶ 99.9%, <45 μm, Alfa Products Inc., Danvers, MA

** 99.99%, <45 μm, Aesar Group, Johnson-Matthey Inc., Seabrook, NH

†† EM 400T, Philips Gloeilampenfabrieken NV, Eindhoven, The Netherlands

§§ Microanalyst-8000, Kevex Corp., Foster City, CA

Based on the dissertation submitted by M.K. Cinibulk for the Ph.D. degree in Material Science and Engineering, University of California, Berkeley, CA 94720

Initially supported by the National Science Foundation under Contract No. DMR 83-1317239. Additional support was provided by the Director, Office of Energy Research, Office of Basic Energy Sciences, Materials Sciences Division of the U.S. Department of Energy under Contract No. DE-AC03-76SF00098. Additional facilities were provided by SRI International.

References

1. S.C. Singhal, "Thermodynamics and Kinetics of Oxidation of Hot-Pressed Silicon Nitride," J. Mater. Sci., **11** 500-09 (1976).

2. D. Cubicciotti, K.H. Lau, and R.L. Jones, "Rate-Controlling Process in the Oxidation of Hot-Pressed Silicon Nitride," J. Electrochem. Soc., **124** [12] 1955-56 (1977).

3. F.F. Lange, S.C. Singhal, and R.C. Kuznicki, "Phase Relations and Stability Studies in the Si_3N_4-SiO_2-Y_2O_3 Pseudoternary System," J. Am. Ceram. Soc., **60** [5-6] 249-52 (1977).

4. I.C. Huseby and G. Petzow, "Influence of Various Densifying Additives on Hot-Pressed Si_3N_4," Powder Metall. Int., **6** [1] 17-19 (1974).

5. K.S. Mazdiyasni and C.M. Cooke, "Consolidation, Microstructure, and Mechanical Properties of Si_3N_4 Doped with Rare-Earth Oxides," J. Am. Ceram. Soc., **57** [12] 536-37 (1974).

6. H.F. Priest, G.L. Priest, and G.E. Gazza, "Sintering of Si_3N_4 under High Nitrogen Pressure," J. Am. Ceram. Soc., **60** [1-2] 81 (1977).

7. F.F. Lange, "Si_3N_4-Ce_2O_3-SiO_2 Materials: Phase Relations and Strength," Am. Ceram. Soc. Bull., **59** [2] 239-40, 49 (1980).

8. G.N. Babini, A. Bellosi, and P. Vincenzini, "Oxidation of Silicon Nitride Hot-Pressed with Ceria," J. Am. Ceram. Soc., **64** [10] 578-84 (1981).

9. W.A. Sanders and D.M. Mieskowski, "Strength and Microstructure of Sintered Si_3N_4 with Rare-Earth-Oxide Additions," J. Am. Ceram. Soc., **64** [2] 304-09 (1985).

10. D.M. Mieskowski and W.A. Sanders, "Oxidation of Silicon Nitride Sintered with Rare-Earth Oxide Additions," J. Am. Ceram. Soc., **68** [7] C-160-63 (1985).

11. E.Tani, S. Umebayashi, K. Kishi, K. Kobayashi, and M. Nishijima, "Gas-Pressure Sintering of Si_3N_4 with Concurrent Addition of Al_2O_3 and 5 wt% Rare Earth Oxide: High Fracture Toughness Si_3N_4 with Fiber-Like Structure," Am. Ceram. Soc. Bull., **65** [9] 1311-15 (1986).

12. N. Hirosaki, A. Okada, and K. Matoba, "Sintering of Si_3N_4 with the Addition of Rare-Earth Oxides," J. Am. Ceram. Soc., **71** [3] C-144-47 (1988).

13. J.E. Shelby and J.T. Kohli, "Rare-Earth Aluminosilicate Glasses," J. Am. Ceram. Soc., **73** [1] 39-42 (1990).

14. J. Ito and H. Johnson, "Synthesis and Study of Yttrialite," Am. Minerologist, **53** 1940-52 (1968).

15. J. Felsche, "Polymorphism and Crystal Data of the Rare-Earth Disilicates of the Type $RE_2Si_2O_7$," J. Less-Common Metals, **21** 1-14 (1970).

16. R.R. Wills, R.W. Stewart, J.A. Cunningham, and J.M. Wimmer, "The Silicon Lanthanide Oxynitrides," J. Mater. Sci., **11** 749-59 (1976).

17. M.K. Cinibulk, G. Thomas, and S.M. Johnson, "$RE_2Si_2O_7$-Si_3N_4 Ceramics: II, Oxidation Behavior," J. Am. Ceram. Soc., this issue (1992).

18. M.K. Cinibulk, G. Thomas, and S.M. Johnson, "$RE_2Si_2O_7$-Si_3N_4 Ceramics: III, Strength and Creep Behavior," J. Am. Ceram. Soc., this issue (1992).

19. R. Raj and F.F. Lange, "Crystallization of Small Quantities of Glass (or a Liquid) Segregated in Grain Boundaries," Acta. Metall., **29** 1993-2000 (1981).

20. M.H. Lewis, C.J. Reed, and N.D. Butler, "Pressureless-Sintered Ceramics Based on the Compound Si_2N_2O," Mater. Sci. Eng., **71** 87-94 (1985)

21. M. Ohashi, S. Kanzaki, and H. Tabata, "Processing, Mechanical Properties, and Oxidation Behavior of Silicon Oxynitride Ceramics," J. Am. Ceram. Soc., **74** [1] 109-14 (1991).

22. K. Liddell and D.P. Thompson, "X-ray Diffraction Data for Yttrium Silicates," Br. Ceram. Trans. J., **85** 17-22 (1986).

23. W.E. Lee, C.H. Drummond III, G.E. Hilmas, J.D. Kiser, and W.A. Sanders, "Microstructural Evolution on Crystallizing the Glassy Phase in a 6 wt% Y_2O_3-Si_3N_4 Ceramic," Ceram. Eng. Sci. Proc., **9** [9-10] 1355-66 (1988).

24. M.K. Cinibulk, G. Thomas, and S.M. Johnson, "Grain-Boundary-Phase Crystallization and Strength of Silicon Nitride Sintered with a YSiAlON Glass," J. Am. Ceram. Soc., **73** [6] 1606-12 (1990).

25. D.A. Bonnell, T.-Y. Tien, and M. Rühle, "Controlled Crystallization of the Amorphous Phase in Silicon Nitride Ceramics, J. Am. Ceram. Soc., **70** [7] 460-65 (1987).

26. T.R. Dinger, R.S. Rai, and G. Thomas, "Crystallization Behavior of a Glass in the Y_2O_3-SiO_2-AlN System," J. Am. Ceram. Soc., **71** [4] 236-44 (1988).

27. G.D. Quinn and W.R. Braue, "Secondary Phase Devitrification Effects upon the Static Fatigue Resistance of Sintered Silicon Nitride," Ceram. Eng. Sci. Proc., **11** [7-8] 616-32 (1990).

28. P. Drew and M.H. Lewis, "Microstructures of Silicon Nitride Ceramics During Hot-Pressing Transformations," J. Mater. Sci., **9** 261-69 (1974).

29. T.M. Shaw, "The Crystallization Of Glasses in the Mg-Si-O-N System," Ph.D. Dissertation, University of California at Berkeley (1980).

30. T.M. Shaw, G. Thomas, and R.E. Loehman, "Formation and Microstructure of Mg-Si-O-N Glasses," J. Am. Ceram. Soc., **67** [10] 643-47 (1984).

31. O.L. Krivanek, T.M. Shaw, and G. Thomas, "The Microstructure and Distribution of Impurities in Hot-Pressed and Sintered Silicon Nitrides," J. Am. Ceram. Soc., **62** [11-12] 585-590 (1979).

32. R.E. Loehman, "Preparation and Properties of Yttrium-Silicon-Aluminum Oxynitride Glasses," J. Am.Ceram. Soc., **62** [9-10] 491-94 (1979).

33. W.D. Kingery, "Densification During Sintering in the Presence of a Liquid Phase, I: Theory," J. Appl. Phys., **30** [3] 301-06 (1959).

34. F.F. Lange, "Liquid-Phase Sintering: Are Liquids Squeezed Out From Between Compressed Particles?," J. Am. Ceram. Soc., **65** [2] C-23 (1982).

35. D.R. Clarke and G. Thomas, "Grain Boundary Phases in a Hot-Pressed MgO Fluxed Silicon Nitride," J. Am. Ceram. Soc., **60** [11-12] 491-95 (1977).

36. D.R. Clarke and G. Thomas, "Microstructure of Y_2O_3 Fluxed Hot-Pressed Silicon Nitride," J. Am. Ceram. Soc., **61** [3-4] 114-18 (1978).

37. L.K.V. Lou, T.E. Mitchell, and A.H. Heuer, "Impurity Phases in Hot-Pressed Si_3N_4," J. Am. Ceram. Soc., **61** [9-10] 392-96 (1978).

38. D.R. Clarke, "On the Equilibrium Thickness of Intergranular Glass Phases in Ceramic Materials," J. Am. Ceram. Soc., **70** [1] 15-22 (1987).

39. W. Braue, G. Wötting, and G. Ziegler, "The Impact of Compositional Variations and Processing Conditions on Secondary Phase Characteristics in Sintered Silicon Nitride Materials," pp. 883-96 in Ceramic Microstructures '86: Role of Interfaces, Edited by J.A. Pask and A.G. Evans, Plenum Press, New York, 1987.

40. W.D. Kingery, H.K. Bowen, and U.R. Uhlmann, Introduction to Ceramics, 2nd Edition, Wiley-Interscience, New York, 1976.

41. D.P. Thompson, "Alternative Grain-Boundary Phases For Heat-Treated Si_3N_4 and β´-Sialon Ceramics," Proc. Br. Ceram. Soc., **45** 1-13 (1990).

Table I. Compositions and Densities of Si_3N_4 Ceramics

Material	Composition (mol%)			Density	
	RE_2O_3	SiO_2	Si_3N_4	(g/cm^3)	(%td)
$Y_2Si_2O_7$-Si_3N_4	5.89	11.78	82.33	3.28	99.5
$Sm_2Si_2O_7$-Si_3N_4	6.08	12.16	81.76	3.48	98.0
$Gd_2Si_2O_7$-Si_3N_4	5.74	11.47	82.79	3.51	99.8
$Dy_2Si_2O_7$-Si_3N_4	5.88	11.77	82.25	3.52	99.2
$Er_2Si_2O_7$-Si_3N_4	5.82	11.64	82.54	3.52	98.5
$Yb_2Si_2O_7$-Si_3N_4	5.91	11.82	82.27	3.59	99.6

Table II. Phases Identified by X-ray Diffraction

Rare-Earth Oxide Additive	Primary Phase	Secondary Phase	Minor Phase
Y_2O_3	β-Si_3N_4	β-$Y_2Si_2O_7$	Si_2ON_2
Sm_2O_3	β-Si_3N_4	A-$Sm_2Si_2O_7$	Si_2ON_2
Gd_2O_3	β-Si_3N_4	δ-$Gd_2Si_2O_7$	Si_2ON_2
Dy_2O_3	β-Si_3N_4	α-, δ-$Dy_2Si_2O_7$	Si_2ON_2
Er_2O_3	β-Si_3N_4	β-$Er_2Si_2O_7$	Si_2ON_2
Yb_2O_3	β-Si_3N_4	β-Yb_2Si_2O7	Si_2ON_2

Figure Captions

Figure 1. Phase relations in the Si_3N_4-SiO_2-Y_2O_3 system, after Lange et al.[3]

Figure 2. Transmission electron micrographs of the six $RE_2Si_2O_7$-Si_3N_4 materials.

Figure 3. Transmission electron micrographs of $Y_2Si_2O_7$-Si_3N_4 in (a) bright-field and (b) dark-field, obtained using diffracted electrons from the [1 3 2] diffraction pattern of β-$Y_2Si_2O_7$ shown inset.

Figure 4. (a) Bright-field image and (b) dark-field image of $Y_2Si_2O_7$-Si_3N_4, obtained using electrons incoherently scattered by the residual amorphous phase; this phase is in bright contrast.

Figure 5. Transmission electron micrographs of (a) $Sm_2Si_2O_7$-Si_3N_4 and (b) $Er_2Si_2O_7$-Si_3N_4 imaged in dark-field using a diffracted beam from the *A*-$Sm_2Si_2O_7$ and β-$Er_2Si_2O_7$ diffraction patterns, respectively.

Figure 6. (a) Bright-field image of Fe-rich inclusions in $Yb_2Si_2O_7$-Si_3N_4. (b) EDS spectrum of Fe-rich inclusion. Ar, Mo, and Cu are present as artifacts of specimen preparation.

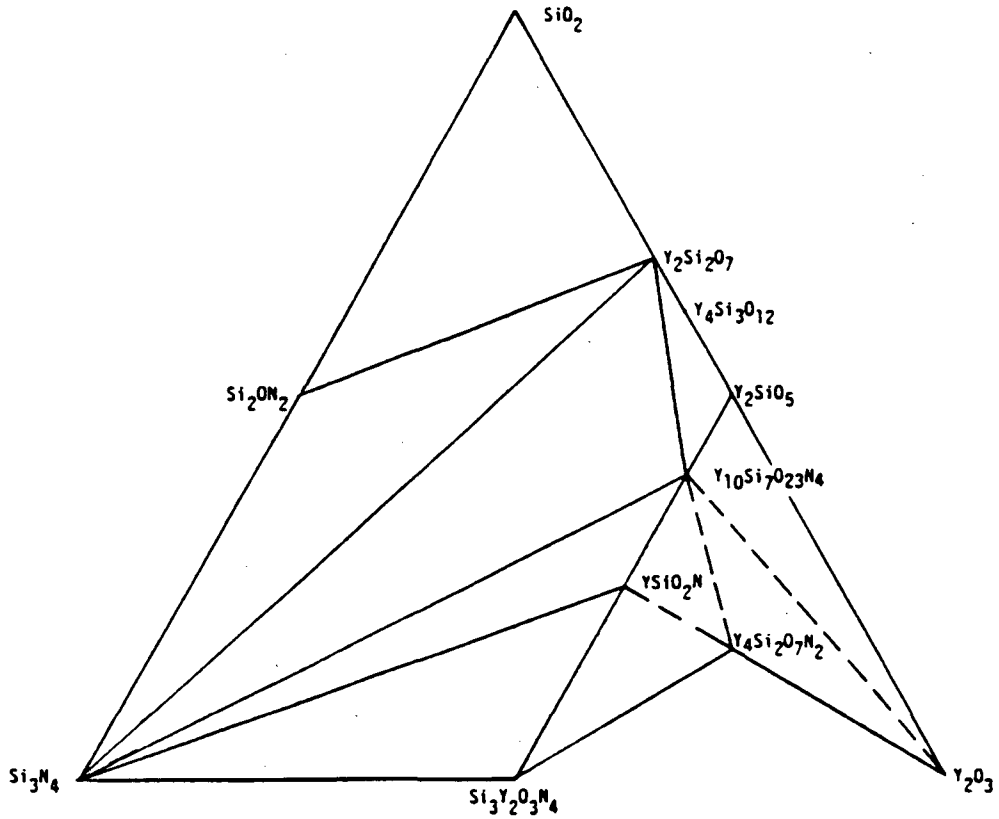

XBL 917-1588

Figure 1

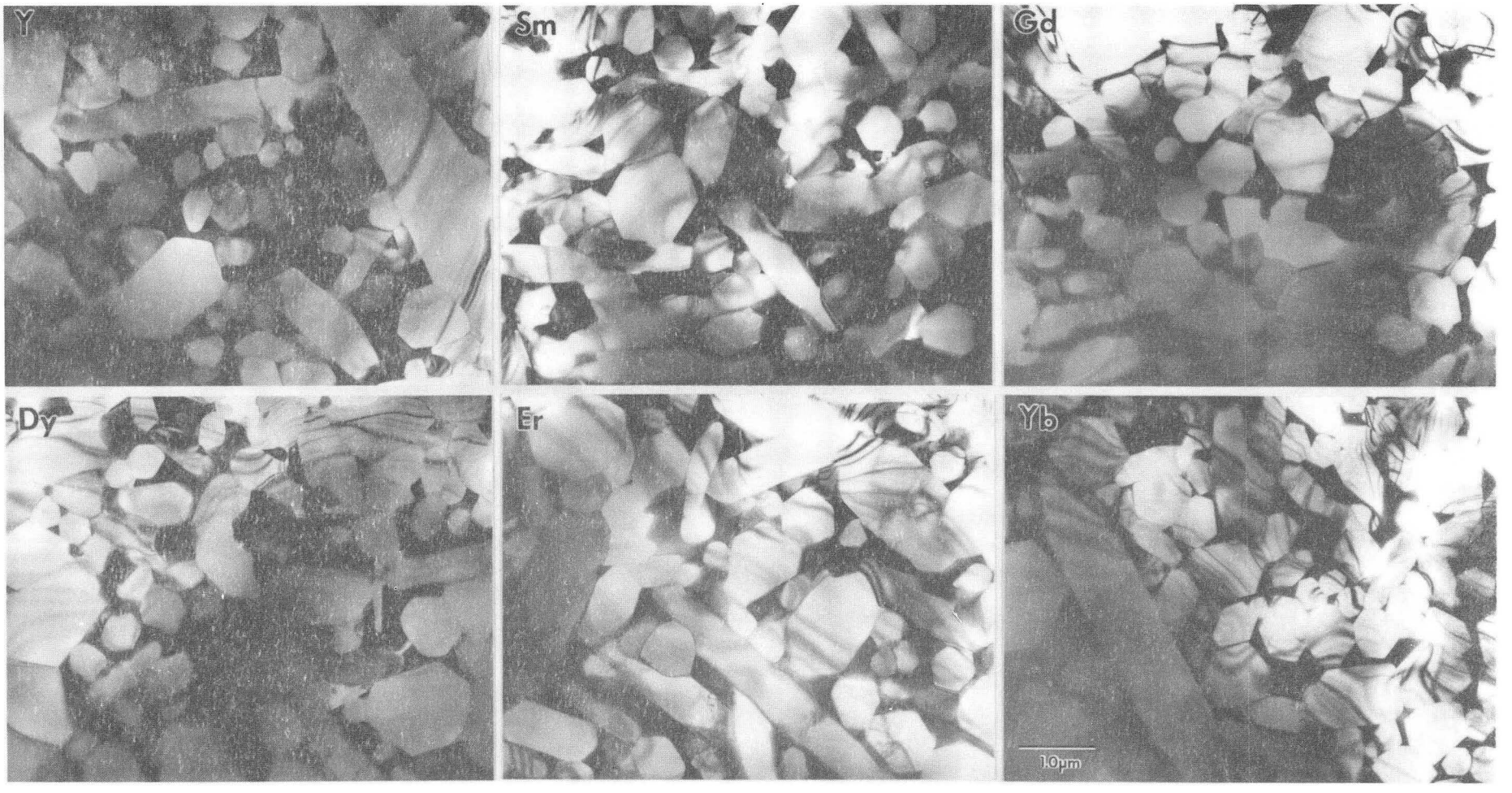

XBB 900-9880

Figure 2

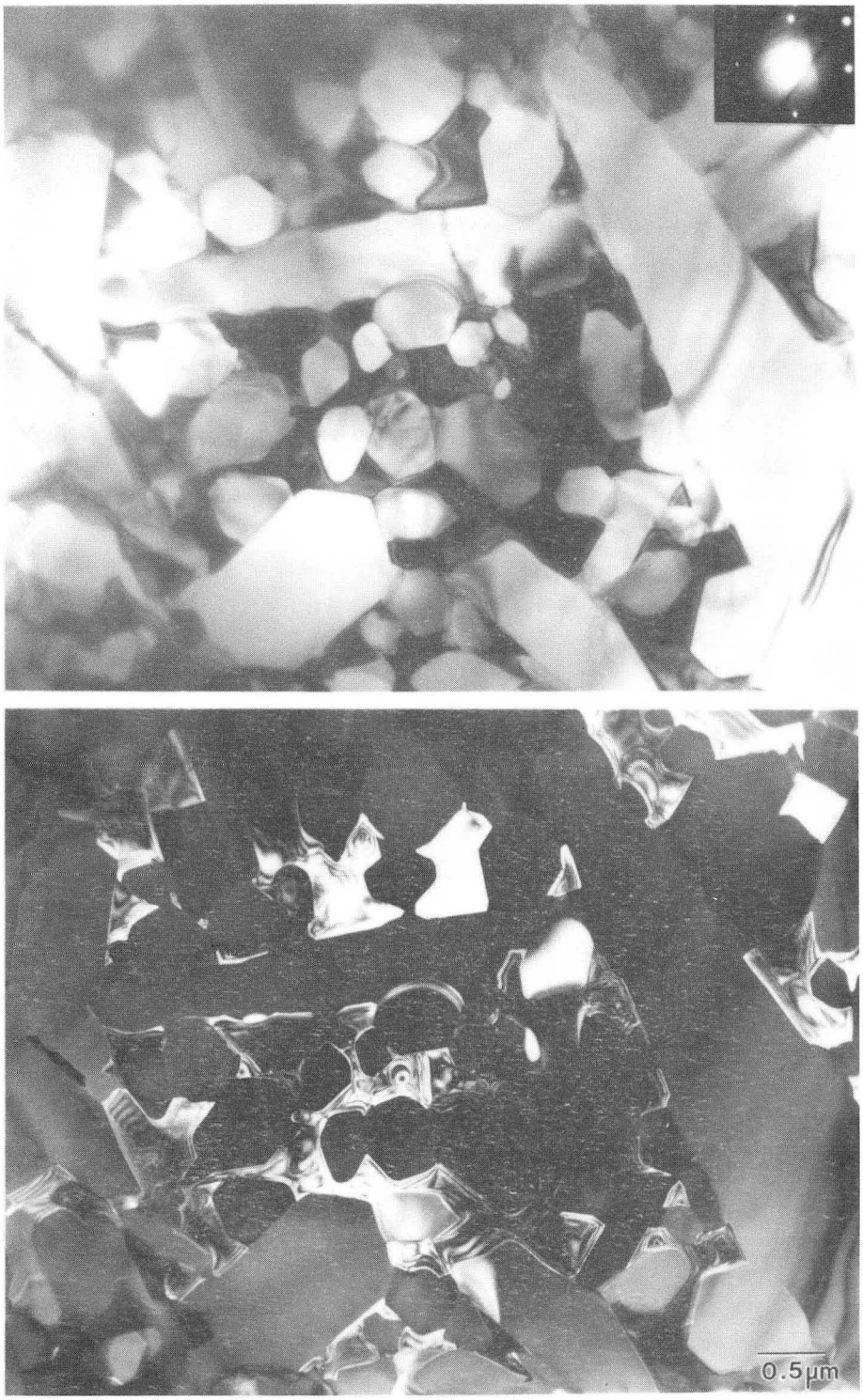

XBB 917-5647

Figure 3

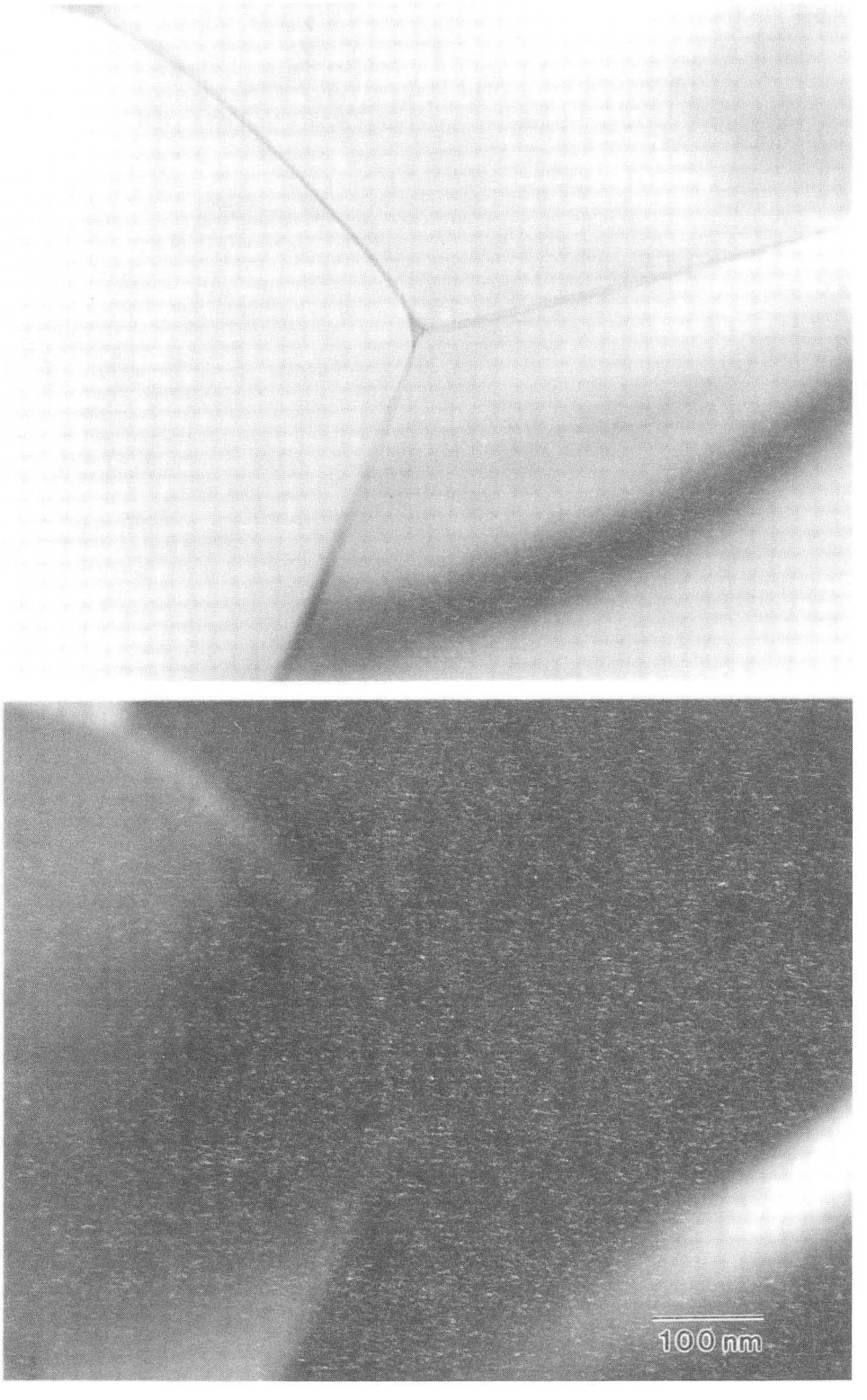

XBB 917-5649

Figure 4

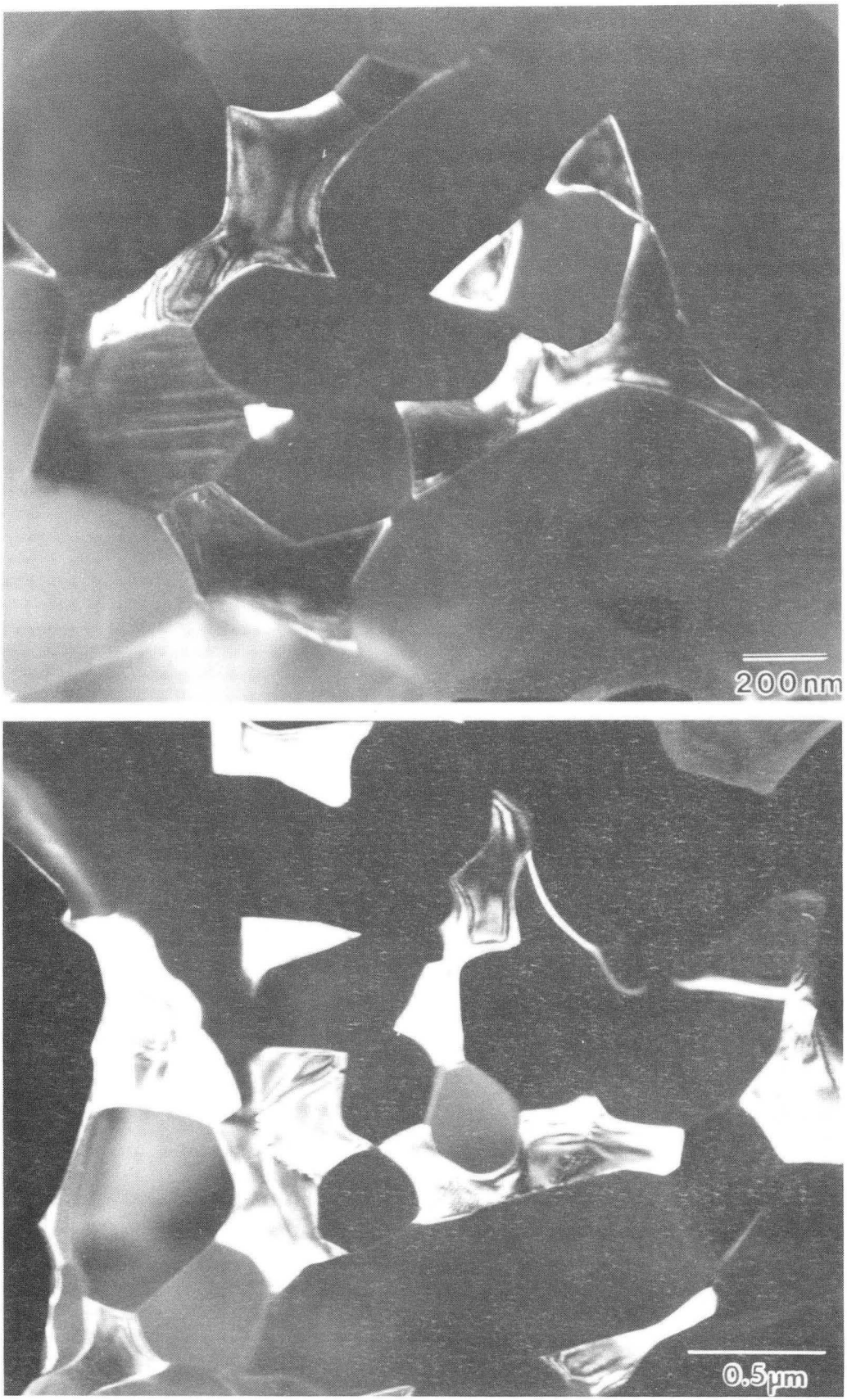

XBB 918-6293

Figure 5

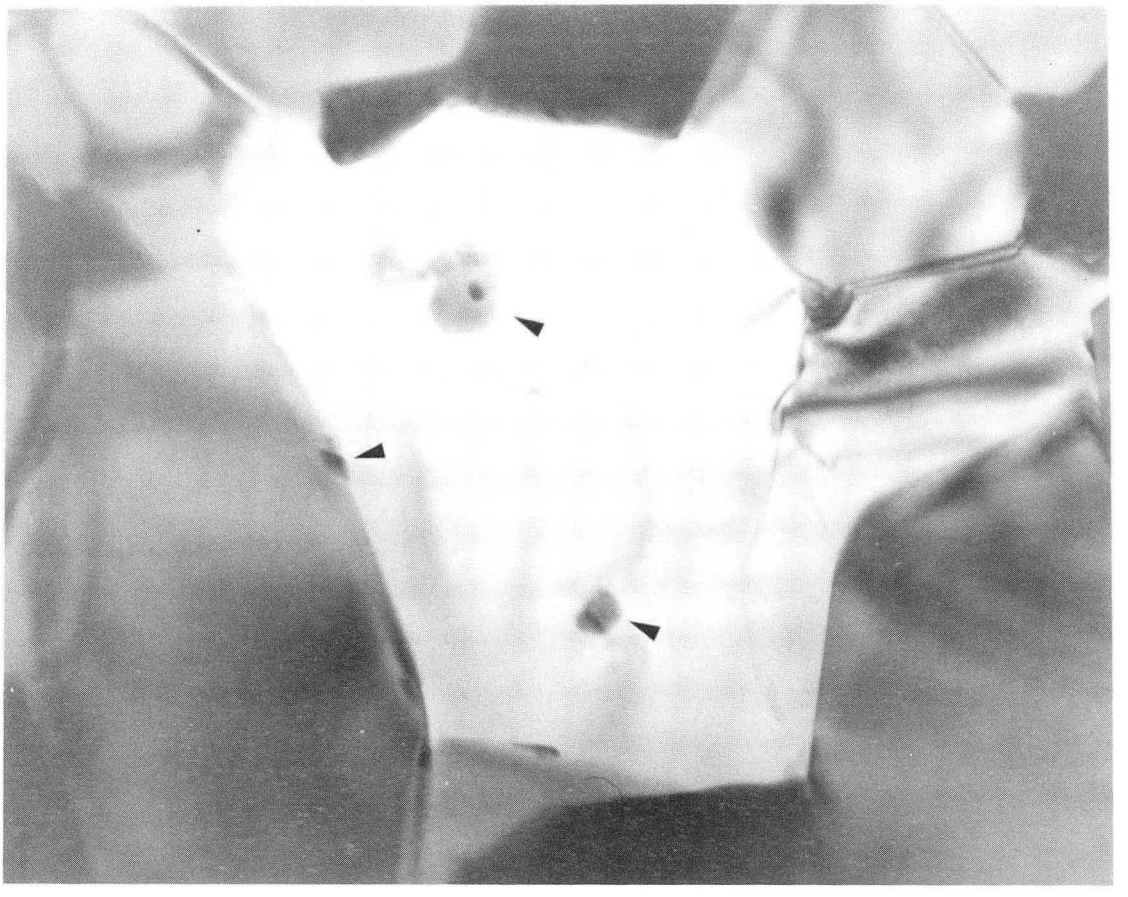

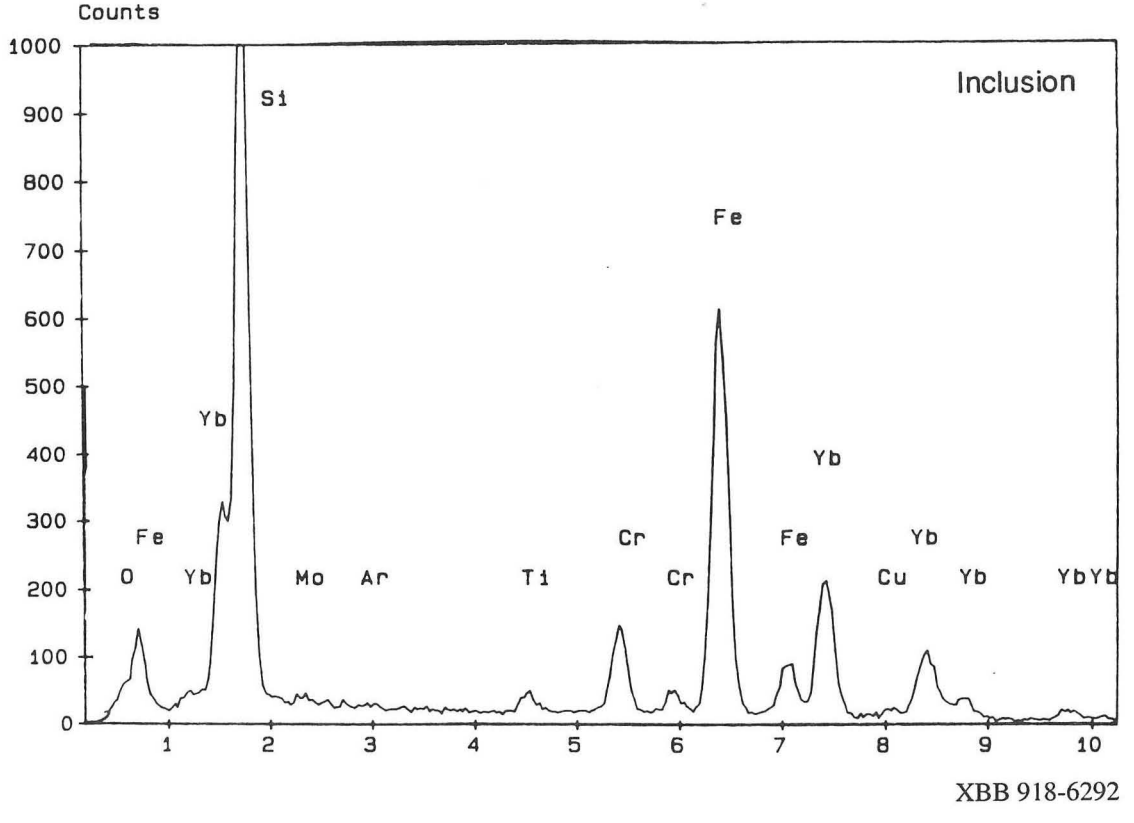
Counts
1000
900
800
700
600
500
400
300
200
100
0
Inclusion
Si
Fe
Yb
Fe
Yb
O
Yb
Mo
Ar
Ti
Cr
Cr
Fe
Yb
Cu
Yb
YbYb
1
2
3
4
5
6
7
8
9
10
XBB 918-6292

Figure 6

LAWRENCE BERKELEY LABORATORY
UNIVERSITY OF CALIFORNIA
INFORMATION RESOURCES DEPARTMENT
BERKELEY, CALIFORNIA 94720